Available online at www.sciencedirect.com
ScienceDirect
JOURNAL OF RARE EARTHS, Vol. 33, No. 6, Jun. 2015, P. 664
JOURNAL OF RARE EARTHS
www.re-journal.com/en/

Mechanism and kinetics of the $BaMgAl_{10}O_{17}:Eu^{2+}$ alkaline fusion reaction

LIU Yifan (刘一凡)[1], ZHANG Shengen (张深根)[1,2,*], PAN De'an (潘德安)[1], TIAN Jianjun (田建军)[1], LIU Hu (刘 虎)[1], WU Maolin (吴茂林)[1], Alex A. Volinsky[3]

(1. Institute of Advanced Materials & Technology, University of Science and Technology Beijing, Beijing 100083, China; 2. Institute of Applied Chemistry, Xinjiang University, Urumqi 830046, China; 3. Department of Mechanical Engineering, University of South Florida, Tampa FL 33620, USA)

Received 9 September 2014; revised 6 April 2015

Abstract: Knowledge of the kinetics and mechanism of $BaMgAl_{10}O_{17}:Eu^{2+}$ (BAM) fusion with sodium hydroxide will benefit recycling rare earth elements (REEs) from the waste phosphors. The reaction temperature range of 290–375 °C and the reaction mechanism were determined using X-ray diffraction, scanning electron microscopy and differential scanning calorimetry. Activation energy was determined by the four model-free methods, and calculated results showed that the Kissinger method value of 579.5 KJ/mol was close to the average value of the Kissinger-Akahira-Sunose (KAS) and the Flynn-Wall-Ozawa (FWO) methods of 563.5 kJ/mol. The calculated activation energy variation tendency versus conversion factor agreed with the proposed mechanism.

Keywords: $BaMgAl_{10}O_{17}:Eu^{2+}$; alkaline fusion; thermo-kinetic analysis; reaction mechanism; rare earths

Waste phosphor has been gaining more attention due to large amounts of rear earth elements (REEs) in it, which can be recycled[1,2]. In 2010, the U.S. Department of Energy assessed six rare earth metals: dysprosium, neodymium, terbium, europium and yttrium, along with indium, as most critical in the short term. Eu^{2+} activated barium magnesium aluminate blue phosphor ($BaMgAl_{10}O_{17}:Eu^{2+}$, BAM) is widely used for plasma display panels and fluorescent lamps due to its high efficiency and excellent color characteristics[3]. The waste phosphor containing BAM has been an important focus in the field of renewable rare earth resources[4]. The alkaline fusion of waste phosphors as a pretreatment process makes it possible to increase the leaching rate of REEs in manufacturing[5,6]. Hence, the knowledge of kinetics and mechanisms of BAM and pure phosphor extraction via fusion with sodium hydroxide will be beneficial for recycling REEs from waste phosphors. However, the reaction mechanisms of BAM alkaline fusion currently remain unknown.

Analytical techniques, such as differential scanning calorimetry (DSC) can be used to determine kinetic parameters of the alkaline fusion reaction[7]. Kinetic parameters are obtained from the DSC data by using either model-fitting or model-free methods. When the reaction mechanism of the alkaline fusion cannot be determined, model-free methods offer a simple and powerful tool to estimate the activation energy by using the data from a series of experiments at different heating rates[8]. The use of the iso-conversion methods is a trustworthy way of obtaining reliable and consistent kinetic information from both non-isothermal and isothermal data. It can also help revealing the complexity of multiple reactions due to the relationship between the activation energy and the conversion factor[9,10].

In this study, a series of alkaline fusion of BAM was investigated by X-ray diffraction (XRD), scanning electron microscopy (SEM) and DSC, and the reaction characteristics were studied under inert conditions at different heating rates of 3, 10, 20, and 30 ºC/min. The purpose of the study was to elucidate the reaction mechanism and reaction kinetics of the alkaline fusion of BAM. Kinetic parameters of the alkaline fusion could be obtained via the four model-free methods, i.e., the Kissinger, the Kissinger-Akahira-Sunose (KAS), the Flynn-Wall-Ozawa (FWO), and the Friedman methods.

1 Materials and methods

1.1 $BaMgAl_{10}O_{17}:Eu^{2+}$ (BAM) alkaline fusion

BAM powder used in this study was obtained from the Dalian Luminglight Co. in Liaoning Province, China. The powder has a particle size of 2–4 μm. BAM powder was mixed with sodium hydroxide following the NaOH/BAM mass ratio of 1:1 by ball-milling.

Foundation item: Project supported by the National Natural Science Foundation of China (U1360202, 51472030), the National Hi-tech R & D Program of China (2012AA063202), the National Key Project of the Scientific & Technical Support Program of China (2011BAE13B07, 2012BAC02B01, 2011BAC10B02), the Fundamental Research Funds for the Central Universities (FRF-TP-14-043A1), the China Postdoctoral Science Foundation (2014M560885), and the Beijing Nova Program (Z141103001814006)

* **Corresponding author:** ZHANG Shengen (**E-mail:** zhangshengen@mater.ustb.edu.cn; **Tel.:** +86-10-62333375)

DOI: 10.1016/S1002-0721(14)60468-3

The mixtures were placed into 200 mL nickel crucibles, and then fusion was performed in a furnace at 150, 200, 250, 300, 325, 350 and 375 ℃ for 2 h. After the reaction the crucibles were immediately placed in water to cool the products. Then the fusion products obtained at 300, 325, 350 and 375 ℃ were cleaned with deionized water several times at 60 ℃ under stirring (200 r/min) for 20 min. After filtration, the products were dried, and ground to a size smaller than 52 μm (270 mesh) for XRD (Philips APD-10 X-ray diffractometer) and SEM (FEI-Quanta250, USA) analysis.

In order to understand the isothermal reaction mechanism, the fusion of the mixtures was performed at 375 ℃ for 30, 60, 90, 120 min, respectively. The products were processed using the same procedure as mentioned above for the XRD and SEM.

DSC was performed using a NETZSH STA 409 C/CD thermal analyzer. The reference material was α-Al_2O_3 powder. Non-isothermal experiments were carried out at heating rates of 3, 10, 20 and 30 ℃/min with the temperature ranging from ambient to 700 ℃.

1.2 Kinetic evaluation using the model-free methods

The general non-isothermal decomposition reaction rate is:

$$\frac{\mathrm{d}\alpha}{\mathrm{d}t} = f(T)\cdot f(\alpha) \tag{1}$$

where α is the conversion factor; t is the reaction time; T is the absolute temperature; $f(\alpha)$ is a differential form of the reaction model, which is a function of α:

$$\alpha = \frac{H_T}{H_S} \tag{2}$$

H_T is the absolute integral area of the DSC curve from the reaction start to temperature T and H_S is the absolute integral area of the DSC curve for the whole selected reaction temperature range.

According to the Arrhenius equation, $f(T)$ is:

$$f(T) = Ae^{-\frac{E}{RT}} \tag{3}$$

where A is the frequency factor, E is the activation energy and R is the universal gas constant. $g(\alpha)$ is the integral form of the reaction model:

$$g(\alpha) = \int_0^{\alpha} \frac{\mathrm{d}\alpha}{f(a)} \tag{4}$$

Model-free methods allow evaluating kinetic parameters without preselecting a reaction model. In this study, the Kissinger, KAS, FWO, and the Friedman methods were selected because they have been successfully applied previously to study solid decomposition[11].

The Kissinger equation can be expressed as Eq. (5)[12]. According to the Kissinger method, the activation energy, E can be obtained from the slope of the plot of $\ln(\beta/T_p^2)$ against $1/T_p$ at different heating rates for a series of experiments, in which T_p is the peak temperature of the DSC curve in the reaction range, and β is the heating rate:

$$\ln\left(\frac{\beta}{T_p^2}\right) = \ln\left(\frac{AR}{E}\right) - \frac{E}{RT_p} \tag{5}$$

The KAS equation can be expressed as Eq. (6)[13]. The activation energy, E, can be obtained from a plot of $\ln(\beta/T^2)$ against $1/T$ for a given value of α:

$$\ln\left(\frac{\beta}{T^2}\right) = \ln\left(\frac{AR}{Eg(\alpha)}\right) - \frac{E}{RT} \tag{6}$$

The FWO equation can be expressed as Eq. (7)[14,15]. The activation energy, E, can be obtained from a plot of $\lg\beta$ against $1/T$ for a given value of α:

$$\lg\beta = \lg\left(\frac{AE}{Rg(\alpha)}\right) - 2.315 - 0.4567\frac{E}{RT} \tag{7}$$

The Friedman equation can be expressed as Eq. (8)[16]. The activation energy, E, can be obtained from a plot of $\ln(\mathrm{d}\alpha/\mathrm{d}t)$ against $1/T$ for a given value of α:

$$\ln\left(\frac{\mathrm{d}\alpha}{\mathrm{d}t}\right) = \ln\left(\beta\frac{\mathrm{d}\alpha}{\mathrm{d}T}\right) = \ln A + \ln f(\alpha) - \frac{E}{RT} \tag{8}$$

2 Results and discussion

2.1 Reaction mechanism

The overall chemical reaction, which takes place during the alkaline fusion of BAM can be described by the following reaction[5]:

$$Ba_{0.9}MgAl_{10}O_{17}:Eu^{2+}_{0.1} + 10NaOH + 0.9CO_2 + 0.025O_2 \rightarrow 10NaAlO_2 + MgO + 0.9BaCO_3 + 0.05Eu_2O_3 + 5H_2O \tag{i}$$

2.1.1 Non-isothermal reaction mechanism

DSC curves of the alkaline fusion at different heating rates are shown in Fig. 1. There were two obvious endothermic peaks before 290 ℃, mainly due to moisture and CO_2 absorbed in NaOH. The first endothermic peak before 100 ℃ was due to the evaporation of water, which was absorbed by NaOH. Similar DSC peaks from water evaporation were often observed in many other endothermic reactions, such as alkaline hydrolysis and ther-

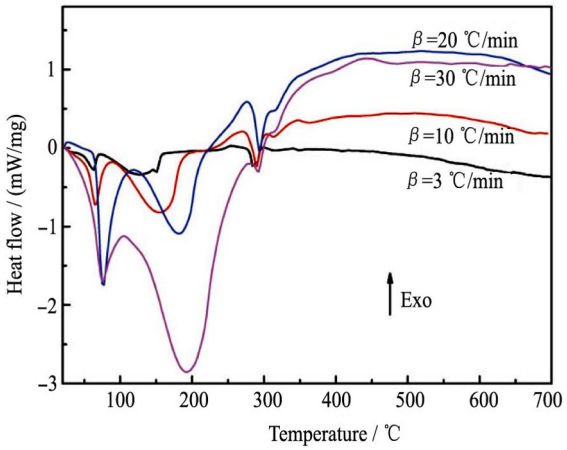

Fig. 1 DSC curves of BAM alkaline fusion reaction at different heating rates

mal decomposition[11,17].

The second endothermic peak between 100 and 290 ºC indicates huge heat absorption during this stage. However, before analyzing the reaction in this temperature range, it is essential to notice certain things. The amount of DSC sample for alkaline fusion was quite small (10 mg), and powder particles had a small size (2–4 μm), thus the sample had a large contact area with air. NaOH is easily moisturized and reacts with CO_2 when exposed to air. This will obviously affect the DSC curve trends.

Alkaline fusion at 150, 200 and 250 ºC was performed to study the reaction behavior. The products were ground and sieved for XRD, and the results are shown in Fig.2. Compared with the XRD pattern of pure blue phosphor (raw material), it is clear that BAM has almost not changed in the alkaline environment at 150–250 ºC, and the Na_2CO_3 phase is observed in all three patterns.

Based on the above analysis, possible reactions, which could take place in the 100–290 ºC range are listed as reactions (ii-iv). $NaHCO_3$ is unstable and can be easily decomposed when heated, and its decomposition through reaction (iv) needs a lot of heat. Because of the very small quantity of the DSC sample, as well as the excess NaOH in the sample, the heat change derived from $NaHCO_3$ between 100 and 290 ºC was mainly represented as the second endothermic peak seen in Fig. 1.

$$2NaOH+CO_2 \rightarrow Na_2CO_3+H_2O \quad (ii)$$

$$Na_2CO_3+H_2O+CO_2 \rightarrow 2NaHCO_3 \quad (iii)$$

$$2NaHCO_3 \rightarrow Na_2CO_3+H_2O+CO_2 \quad (iv)$$

In the XRD pattern of the non-washed fusion products at 300–375 ºC (not listed), sodium metaaluminate salts were detected as the main phase, while other phases could not be clearly recognised. Thus, once the BAM starts to react with NaOH, a large amount of $NaAlO_2$ will be produced. This also indicates that the reaction of BAM alkaline fusion began at about 300 ºC.

Fig. 3 shows XRD patterns of the alkaline fusion products at 300, 325, 350 and 375 ºC. All of these four products were washed by deionized water to avoid the effect of $NaAlO_2$. A significant reduction of BAM peaks

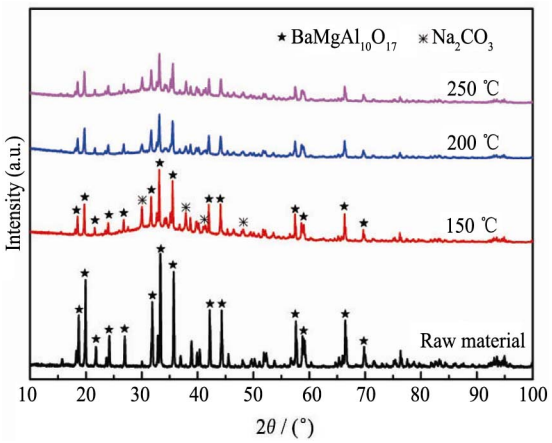

Fig. 2 XRD patterns of BAM alkaline fusion products at 150, 200, 250 ºC and raw material

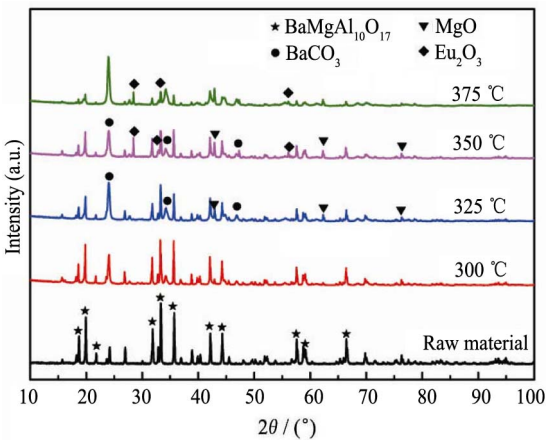

Fig. 3 XRD patterns of the washed BAM alkaline fusion products at 300, 325, 350 and 375 ºC

intensity was observed from 300 to 325 ºC, however, the main phase was still BAM. When the temperature reached 325 ºC, MgO and $BaCO_3$ were observed. A small but obvious Eu_2O_3 phase could also be observed at 325 ºC. The diffraction peaks attributed to the BAM phase became weaker as the temperature increased, but no new phases were detected in the samples. Until 375 ºC the BAM diffraction peaks almost disappeared, and the main phases were MgO, $BaCO_3$ and Eu_2O_3. BAM was decomposed completely at 375 ºC and no changes could be observed at higher temperatures.

Fig. 4 shows SEM micrographs of BAM alkaline fusion products at 300, 325, 350, 375 ºC and the raw BAM. The raw material is in the form of irregular 3–5 μm particles with smooth surface in Fig. 4(a). Most particles retained their basic shape after alkaline fusion at 300 ºC, but many parallel gullies were observed on the surface of particles, as seen in Fig. 4(b). These gullies were formed mainly due to hot alkaline corrosion. From the start of BAM fusion (about 290 ºC) to 320 ºC, aluminum oxide in BAM reacted with NaOH preferentially and generated partial aluminate. These gullies in Fig. 4(b) may be produced because of this preferential reaction. When alkaline fusion occurred at 325 and 350 ºC, BAM particles were decomposed into small agglomerated grains in Fig. 4(c) and (d). When the temperature increased to 375 ºC, as seen in Fig. 4(e), no particle size change was observed. Based on the above XRD analysis, at 320–375 ºC, MgO, $BaCO_3$ and Eu_2O_3 were present in the products. These small particles agglomerated in the alkaline environment, and after washing were seen as morphological features in Figs. 4(c), (d) and (e). It could be confirmed that BAM alkaline fusion finished at about 375 ºC. These results are in agreement with the DSC curves in Fig. 1.

Eq. (v–viii) represent possible reactions in the temperature range of 290–375 ºC. The solid state reaction is difficult to occur, and the essence of the reaction is the oxide transfer. Based on this theory, reactants were simply rewritten as oxides forms, to illustrate the reaction

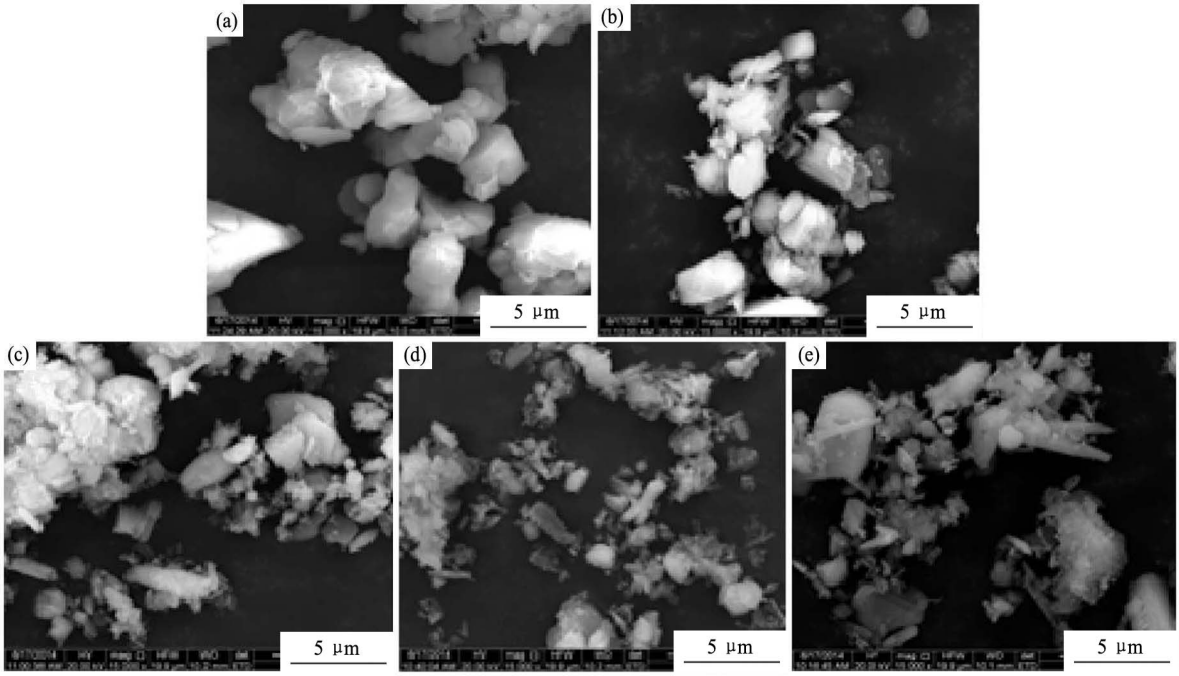

Fig. 4 SEM micrographs of BAM alkaline fusion products at different temperatures
(a) Raw BAM; (b) 300 °C; (c) 325 °C; (d) 350 °C; (e) 375 °C

process more simply and clearly.

Eq. (v) represents the preferential reaction mentioned above in Fig. 4, which most likely takes place in the 290–320 ºC range. In reaction (v), $BaMgAl_{10}O_{17}$ was re-written as $BaO{\cdot}MgO{\cdot}(Al_2O_3)_5$ and NaOH as $Na_2O{\cdot}H_2O$. In the crystal structure of $BaMgAl_{10}O_{17}:Eu^{2+}$, Eu ions were considered as doped ions, which replace the position of Ba[18,19]. It could be speculated that the reaction behavior of Eu is similar to the reaction behaviour of Ba. Rewritting $BaMgAl_{10}O_{17}:Eu^{2+}$ as $EuO{\cdot}BaO{\cdot}MgO{\cdot}(Al_2O_3)_5$, reaction (v) was changed to (vi). When the temperature was higher than 320 ºC, in the NaOH alkaline environment, barium ions could not exist as barium oxide. United with CO_2, barium ions transfer to a very stable form of $BaCO_3$. While europium and magnesium ions will exist in the form of oxides under high temperature alkaline enveironment, these oxides would not change during the cooling process. Bivalent europium was easily oxdized into the trivalent europium, represented by reaction (viii).

$$BaO{\cdot}MgO{\cdot}(Al_2O_3)_5+5Na_2O{\cdot}H_2O\rightarrow BaO{\cdot}MgO+10NaAlO_2+5H_2O \quad (v)$$

$$EuO{\cdot}BaO{\cdot}MgO{\cdot}(Al_2O_3)_5+5Na_2O{\cdot}H_2O\rightarrow EuO{\cdot}BaO{\cdot}MgO+10NaAlO_2+5H_2O \quad (vi)$$

$$EuO{\cdot}BaO{\cdot}MgO+CO_2\rightarrow EuO+BaCO_3+MgO \quad (vii)$$

$$2EuO+1/2O_2\rightarrow Eu_2O_3 \quad (viii)$$

2.1.2 Isothermal reaction mechanism

In order to identify the reaction mechanism of BAM alkaline fusion under constant temperature, the fusion of the mixtures (BAM:NaOH=1:1, wt.%) was performed for 30, 60, 90, 120 min, respectively, at 375 ºC, at which temperature BAM may be decomposed completely. The products were washed by deionized water to avoid the effect of $NaAlO_2$. XRD and SEM results are shown in Figs. 5 and 6.

With more time, significant reduction of BAM peaks is observed in Fig. 5. Until 120 min, the BAM phase nearly disappeared. When the reaction was performed for 30 min, only MgO was detected, except for BAM. While for 60 and 90 min, MgO and $BaCO_3$ were observed. Obvious Eu_2O_3 was observed in the products reacted for 120 min. The trend of the isothermal reaction at 375 ºC is similar to the trend of non-isothermal reaction as discussed in section 2.1.1.

SEM micrographs of the fusion products held for different time are shown in Fig. 6. When the fusion reaction was performed for 30 min, many obvious parallel gullies were observed on the surface of the BAM particles, and this phenomenon was similar to the results seen in Fig. 4(b). With the holding time increasing to 60 and 90 min,

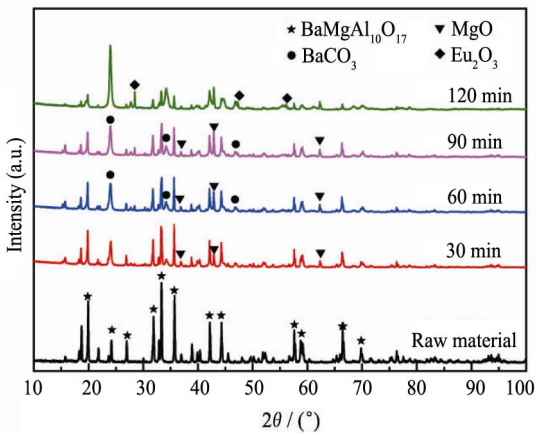

Fig. 5 XRD patterns of BAM alkaline fusion products washed for different time

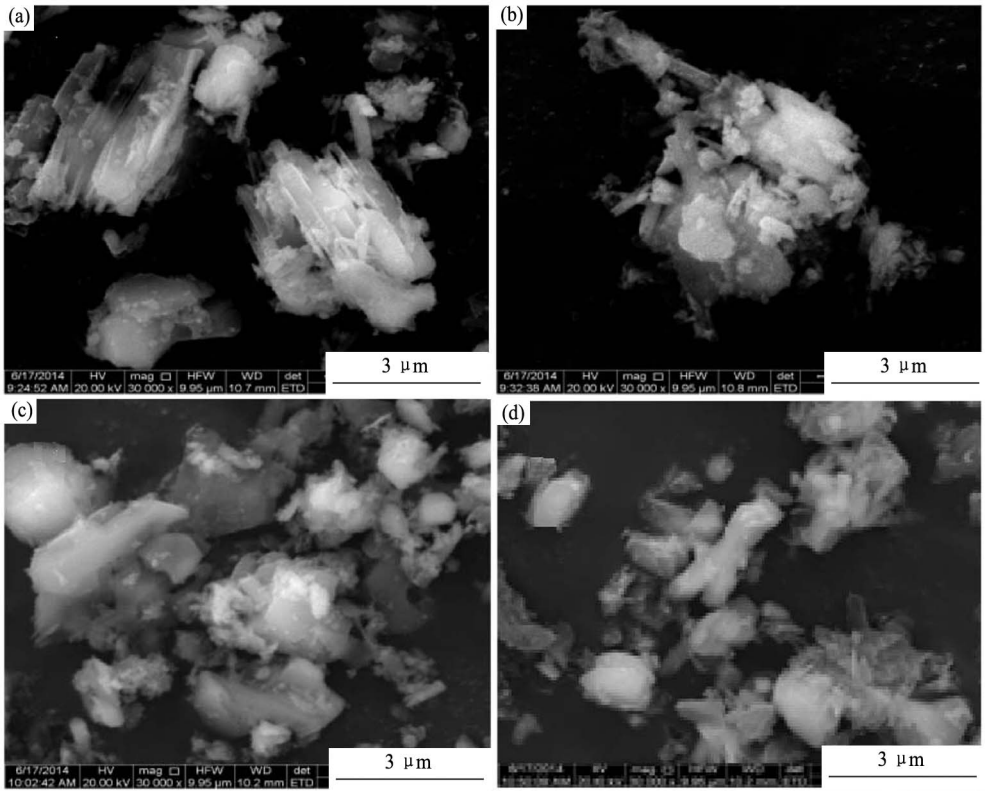

Fig. 6 SEM micrographs of BAM alkaline fusion products held at 375 ºC for different time
(a) 30 min; (b) 60 min; (c) 90 min; (d) 120 min

the products appeared as small agglomerated particles in Fig. 6(b) and (c). This indicates that BAM was composed of small particles. In Fig. 6(d), small agglomerated particles were also observed. The trend for the morphology variation in Fig. 6 is very similar with the trend in Fig. 4.

Combined with the XRD analysis of the isothermal reaction products, it can be concluded that for BAM alkaline fusion, non-isothermal reaction (290–375 ºC) and isothermal reaction (at 375 ºC) share similar mechanism. Different reaction time under the same reaction temperature affects only the extent of the reaction, but not the intrinsic character of the reaction. Thus, the thermal kinetic parameters calculated from the non-isothermal reaction process could also be used to describe the thermal reaction at the specific temperature.

2.2 Activation energy determination

DSC results were analyzed by using model-free methods to calculate the kinetic parameters. The same conversion factor (0.2–0.9) was used for the DSC curves (290–375 ºC) at different heating rates. Fig. 7 shows the plots used for calculating the activation energy at different conversion factors using different model-free methods (Kissinger, KAS, FWO and Friedman). The detailed results of the activation energy, E, and the coefficients of determination (R^2) are shown in Tables 1 and 2.

The activation energy values increased with the conversion factor, α, in all of the KAS, FWO, and Friedman cases, as seen in Fig. 8. Moreover, the difference between the lowest and the highest activation energy value was 1683.9, 1602.2 and 2285.6 kJ/mol, respectively, for the conversion factor ranging from 0.2 to 0.9. This indicates that the BAM alkaline fusion is a multi-step process. When the conversion factor increased from 0.6 to 0.7, the activation energy increased from 340.5 to 675.2 kJ/mol (KAS), and from 333.5 to 652.0 kJ/mol (FWO). When the conversion factor increased further from 0.8 to 0.9, a sharp increase was observed in both KAS and FWO methods: from 757.9 to 1857.1 kJ/mol (KAS), and from 7307 to 1776.2 kJ/mol (FWO). For the Friedman method, the similar sharp increase (from 958.3 to 2432.3 kJ/mol) was observed when the conversion factor increased from 0.8 to 0.9. With the increased reaction extent, it would be more difficult to activate the reaction, based on the determined activation energy. The increase in the activation energy could be explained by the heat transfer effect at higher temperature[20].

The activation energy values obtained by the Friedman method were higher than that obtained by the KAS and FWO methods. The value of the Kissinger method (579.5 kJ/mol) was close to the average values of the KAS and FWO methods, i.e., 572.7 and 554.3 kJ/mol, respectively.

The variation tendency of the calculated activation energy with the conversion factor clearly shows that the reaction of the BAM alkaline fusion is a multi-step process. This result agrees with the reaction mechanism mentioned above. Thus, the proposed mechanism is confirmed and the calculated results in this paper are credible.

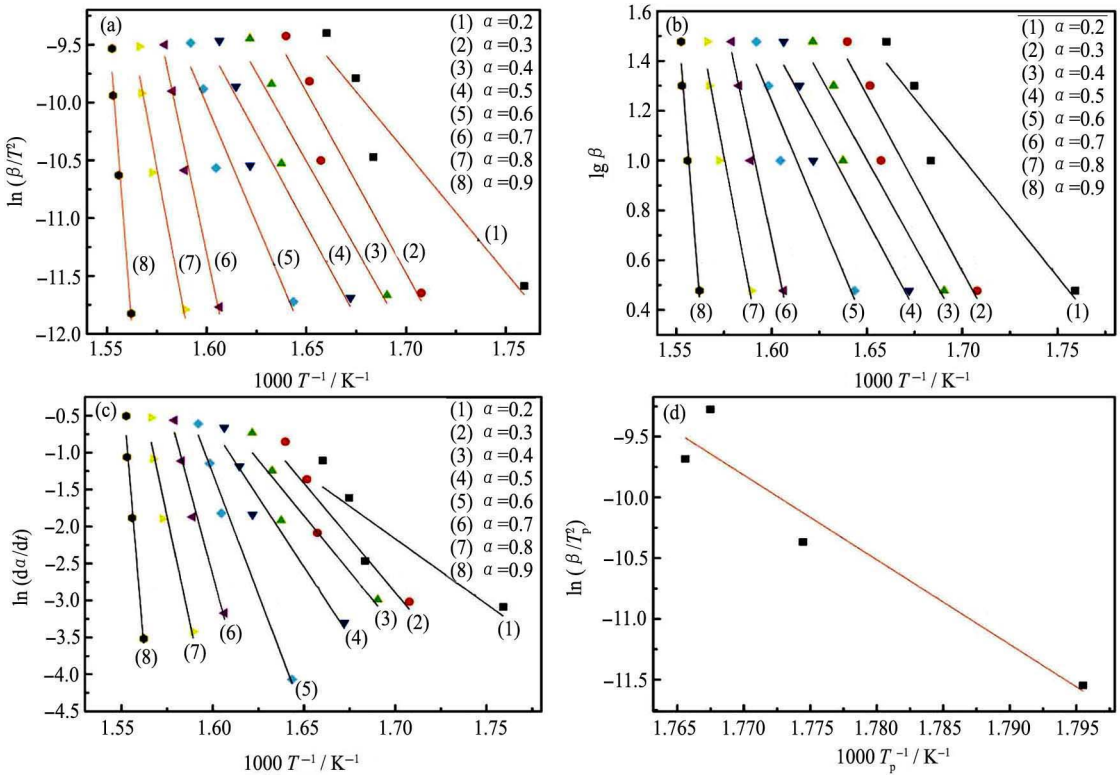

Fig. 7 Plots for calculating the activation energy at different conversion factors, α, by KAS (a), FWO (b), Friedman (c) and Kissinger methods (d)

Table 1 Activation energy calculated by the Kissinger method

Kissinger	*E*/(kJ/mol)	R^2
	579.573	0.88658

Table 2 Activation energy calculated by the KAS, FWO and Friedman methods

α	KAS		FWO		Friedman	
	E/(kJ/mol)	R^2	*E*/(kJ/mol)	R^2	*E*/(kJ/mol)	R^2
0.2	173.2446	0.8877	173.9763	0.8984	146.6817	0.67766
0.3	260.8997	0.90283	257.5339	0.90931	245.4515	0.83265
0.4	253.1939	0.88196	250.3066	0.89005	250.7129	0.85258
0.5	263.7881	0.89492	260.4807	0.90197	313.0022	0.9269
0.6	340.5276	0.90596	333.586	0.91101	542.3901	0.98266
0.7	675.2446	0.97764	652.0408	0.97829	764.8907	0.96677
0.8	757.9103	0.92797	730.7473	0.92983	958.3714	0.92784
0.9	1857.184	0.96001	1776.223	0.96045	2432.36	0.96393

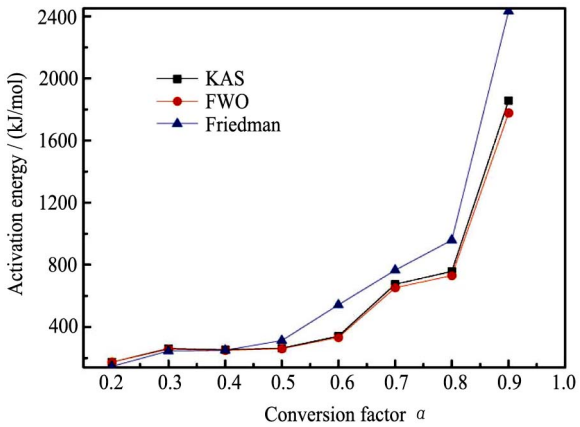

Fig. 8 Activation energy changes with the conversion factor obtained by the KAS, FWO and Friedman methods

3 Conclusions

The reaction temperature of the BAM alkaline fusion ranged from 290 to 375 ℃. Reaction mechanism of both non-isothermal and isothermal reactions was proposed and discussed. The non-isothermal and isothermal processes shared a similar reaction mechanism. Activation energy calculated by the Friedman method was higher than the KAS and FWO methods. The value obtained using the Kissinger method (579.5 kJ/mol) was close to the average values of the KAS and FWO methods, i.e., 572.7 and 554.3 kJ/mol, respectively. Activation energy during the reaction temperature interval had an appropriate value of 563.5 kJ/mol (the average value obtained by the KAS and FWO methods). The variation tendency of the calculated activation energy was consistent with the proposed reaction mechanism.

References:

[1] Curtis N. Rare Earths, We Can Touch Them Everyday. Lynas Presentation at the JP Morgan Australia Corporate Access Days, New York. 2010: 27.

[2] Binnemans K, Jones P T. Perspectives for the recovery of rare earths from end-of-life fluorescent lamps. *J. Rare Earths*, 2014, **32**(3): 195.

[3] Dong Y, Wu Z S, Han X L, Chen R, Gu W J. Preparation of $BaMgAl_{10}O_{17}:Eu^{2+}$ phosphor with small particle size by co-precipitation method. *J. Alloys Compd.*, 2011, **509**: 3638.

[4] Fan Y, Fukiko K, Yuzo B, Noriho K, Masahiro G. Selective extraction and recovery of rare earth metals from phosphor powders in waste fluorescent lamps using an ionic liquid system. *J. Hazard. Mater*., 2013, **254-255**: 79.
[5] Liu H, Zhang S G, Pan D A, Tian J J, Yang M, Wu M L, Alex A V. Rare earth elements recycling from waste phosphor by dual hydrochloric acid dissolution. *J. Hazard. Mater*., 2014, **272**: 96.
[6] Saber D, Lejus A M. Elaboration and characterization of lanthanide aluminate single crystals with the formula $LnMgAl_{11}O_{19}$. *Mater. Res. Bull*., 1981, **16**: 1325.
[7] Supriya N, Catherine K B, Rajeev R. DSC-TG studies on kinetics of curing and thermal decomposition of epoxy-ether amine systems. *J. Therm. Anal. Calorim*., 2013, **112**: 201.
[8] Biagini E, Fantei A, Tognotti L. Effect of the heating rate on the devolatilization of biomass residues. *Thermochim. Acta*, 2008, **472**: 55.
[9] Vyazovkin S, Wight C A. Model-free and model-fitting approaches to kinetic analysis of isothermal and nonisothermal data. *Thermochim. Acta*, 1999, **340**: 53.
[10] Vyazovkin S. Computational aspects of kinetic analysis: Part C. The ICTAC kinetics project—the light at the end of the tunnel? *Thermochim. Acta*, 2000, **355**: 155.
[11] Liang Y G, Cheng B J, Si Y B, Cao D J, Jiang H Y, Han G M, Liu X X. Thermal decomposition kinetics and characteristics of Spartina alterniflora via thermogravimetric analysis. *Renew. Energy*, 2014, **68**: 111.
[12] Homer E K. Reaction kinetics in differential thermal analysis. *Anal. Chem.*, 1957, **29**: 1702.
[13] Akahira T, Sunose T. Joint convention of four electrical institutes. *Res. Rep. Chiba. Inst. Technol*., 1971, **16**: 22.
[14] Flynn J H, Wall L A. A quick, direct method for the determination of activation energy from thermogravimetric data. *J. Poly. Sci. Part B: Polymer Letters*, 1966, **4**: 323.
[15] Ozawa T. A new method of analyzing thermogravimetric data. *Bull. Chem. Soc. Jpn*., 1965, **38**: 1881.
[16] Henry L F. Kinetics of thermal degradation of char-forming plastics from thermogravimetry. Application to a phenolic plastic. *J. Poly. Sci. Part C: Polymer Symposia*, 1964, **6**: 183.
[17] López-Fonseca R, González-Velasco J J, Gutiérrez-Ortiz J I. A shrinking core model for the alkaline hydrolysis of PET assisted by tributylhexadecylphosphonium bromide. *Chem. Eng. J*., 2009, **146**: 287.
[18] Wu Z H, Cormack A N. Defects in $BaMgAl_{10}O_{17}:Eu^{2+}$ blue phosphor. *J. Electroceram.*, 2003, **10**: 179.
[19] Kim K, Kim Y, Chun H, Cho T, Jung J, Kang J. Structural and optical properties of $BaMgAl_{10}O_{17}:Eu^{2+}$ phosphor. *Chem. Mater*., 2002, **14**: 5045.
[20] Thanasit W, Nakorn T. Non-isothermal pyrolysis characteristics of giant sensitive plants using thermogravimetric analysis. *Bioresour. Technol*., 2010, **101**: 5638.